



Journal of Applied and Computational Mechanics



Research Paper

Turbulent Forced Convection and Entropy Generation of Impinging Jets of Water- Al_2O_3 Nanofluid on Heated Blocks

Bouziiane Boudraa^{id}, Rachid Bessaïh^{id}

LEAP Laboratory, Department of Mechanical Engineering, University of Mentouri Brothers -Constantine 1, Route de Ain El Bey, Constantine, 2500, Algeria

Received September 29 2020; Revised November 11 2020; Accepted for publication November 11 2020.

Corresponding author: B. Boudraa (bouziiane.boudraa@umc.edu.dz)

© 2021 Published by Shahid Chamran University of Ahvaz

Abstract. A computational analysis on water- Al_2O_3 nanofluid turbulent forced convection is performed to analyze heat transfer and entropy production in a channel containing heated blocks, cooled by impinging jets. The two phase mixture model (TPMM) is used. This work can be considered as a good contribution to improving thermal performance and enhancing the heat transfer rate (HTR) for some engineering industries. After completing the current study, we concluded that the increase in the Reynolds number (Re) and the volume fraction of nanoparticles (φ), the decrease in spacing between the heated block (D_b) and moving the location of the second jet (J2) to the first jet (J1) contribute to increasing the heat transfer rate (HTR). In addition, the TPMM gives higher values of average Nusselt number \overline{Nu} than the single-phase model (SPM). The thermal ($\dot{S}_{g,th}$), frictional ($\dot{S}_{g,v}$) and total ($\dot{S}_{g,t}$) entropy generation values increase with Re and φ . When D_b is reduced, $\dot{S}_{g,t}$ increases. However, $\dot{S}_{g,t}$ increases when the jet position vary from J2 to J1. Different correlations are proposed for \overline{Nu} . Our results are compared with data available in the literature.

Keywords: Heat transfer, Turbulent flow, entropy generation, nanofluid, impinging jets, heated blocks.

1. Introduction

Increased HTR is an active and important area of engineering research due to its contribution to developing highly efficient cooling technologies to meet ever-growing demand for developing efficient designs for thermal equipment. Various techniques have been proposed in recent years to enhance convective heat transfer [1-4]. In order to improve the HTR in different systems, nanofluid have been used more widely in recent years compared to conventional heat transfer fluids [5-6]. In this regard, one of the most promising strategies for promoting heat transfer compared to conventional forced convection techniques is its liquid jet effect cooling due to its performance the coefficient of heat transfer (h) is higher. As an obvious implication, liquid jets were used in various industrial and engineering applications for example cooling of heat engines, thermal control in high-heat-dissipation electronic devices and thermal treatment of metals and materials processing [7]. Several experimental and numerical studies have been conducted, for example. Menni et al. [8] studied the effect of different base fluid on the HTR. They found that the pure ethylene glycol flows give the largest thermal exchange compared with the water and water- ethylene glycol mixture. Ibrahim and Ahmed [9] investigated numerically the impinging jet's laminar heat transfer with nanofluid. The outcomes demonstrate that the \overline{Nu} , performance factor, $\dot{S}_{g,t}$ increases with increasing φ . Menni et al. [10,11] studied the effect the presence of nanoparticles and baffle plates in a channel, they also examined the effect of different outlet models in baffled channels on the HTR used $\text{Al}_2\text{O}_3\text{-H}_2\text{O}$. A detailed review of the numerical and experimental studies performed to improve the HTR by Menni et al. [12-13]. Abdelrehim et al. [14] studied SPM and TPMM of nanofluid on heat transfer properties. Results show that the TPMM gives higher values of Nu and \overline{Nu} . Sheikholeslami et al. [15-16]. Used TPMM to simulate fluid flow, heat transfer, energy and entropy evaluation inside a tube with enhanced turbulator. Selimefendigil and Özttop [17] investigated numerically the effects of different parameters such as pulse frequency, Re and φ . They showed that in the pulsating flow case, HTR will improve with increasing Re



and ϕ . A numerical study using nanofluids to cool an isothermal hot surface with an adiabatic rotating cylinder was carried out by Selimefendigil and Öztöpe [18]. It was found that the \overline{Nu} increases with Re, but the HTR was higher in the case when the cylinder is closer to the jet inlet. The influences of uniform and non-uniform impact jets velocity were carried out by Izadi et al. [19]. Results indicate that raising the values of ϕ enhances HTR. Additionally, when using non-uniform impingement jet with a low speed distribution, the thermal performance is improved. Lamraoui et al. [20] investigated numerical the flow characteristics of a non-Newtonian Al₂O₃-water nanofluid. It was found that Nu is much higher for non-Newtonian nanofluid than Newtonian flow. Manca et al. [21] analyzed fluid dynamic and thermal behaviors of an enclosed laminar impinging slot jets with nanofluid. Results show that h and Nu values increase with increasing ϕ and Re. Amjadian et al. [22] experimentally studied the properties of the impact jet on a hot surface using Cu₂O-water nanofluid. Results showed that the rise in Re and ϕ increases the h value. Yousefi et al. [23] carried out an experimental study into the impingement of a planar jet on a plate. They showed a decrease in h with an increase in Re from 1732 to 2250, also they found that the use of Al₂O₃ - nanofluid at low ϕ of 0.02% and 0.05% improved h and \overline{h} . Teamah et al. [24] studied numerically and experimentally the behavior of nanofluids flow impingement on horizontal flat plate. They found that increasing ϕ increases h compared to pure water. The heat transfer properties of air/nanofluid jet cooling flux on a rotating hot circular disk, using a multiphase VOF model were studied by Mahdavi et al. [25]. Results showed that Nu values increase with increasing ϕ and disk rotation speed. Sun et al. [26] experimentally studied heat transfer with Cu Nanofluids from single impinging jet. It was found that the coefficient h is higher when using round nozzles compared to square nozzles. Pratap et al. [27] conducted the effect of nanofluids for the enhancement of the HTR by impingement jet. They observed that the Nu values increases with the increase in H/D ratio. A numerical study of the impact jet in a small channel using the Eulerian-Eulerian biphasic method was performed by Venkatasubbaiah and Abhijith [28]. HTR enhancement is 25% for Al₂O₃ - water nanofluid and 60% for Cu-water nanofluid compared to pure water, at Re = 300 and $\phi = 5\%$. Abanti et al. [29] studied the effects of heat transfer properties on a moving plate. They found that the \overline{Nu} significantly rises with Re and with the plate velocity. A numerical simulation in a confined jet was performed by Rahimi-Esbo et al. [30]. Increasing Re, the aspect ratio and ϕ lead to an increase in the values of \overline{Nu} . Results showed that raising the values of Re, aspect ratio and ϕ conducts an increase in values of \overline{Nu} . Youssefi Lavouraki et al. [31] conducted a numerical simulation of confined jet using TPM. The outcomes indicate that Cf and Nu decrease and increase, respectively, with a higher of Re, H/W ratio and ϕ . Youssef Lavouraki et al. [32] investigated the heat transfer on a confined jet. Results indicated that an increase in ϕ contributes to an increase in Nu. Paulraj and Sahu [33] investigated numerically the conjugated heat transfer in laminar impinging jet on various hot sources using different nanofluids. They observed that the conjugate HTR increases with the decrease of nanoparticles diameter. It was also found that Al₂O₃-water nanofluid appears to be higher \overline{Nu} compared to other nanofluids. The fluid flow and heat transfer properties resulting from the cooling of a group of heated blocks in a channel using an air jet was analyzed by Arquis et al. [34]. HTR of the small heated blocks is improved. Lam and Prakash [35] numerically studied heat transfer and \dot{S}_g of heat sources with or without porous media. They showed that \overline{Nu} , $\dot{S}_{g,t}$ and $\dot{S}_{g,v}$ increases with increasing Darcy number, Re and porous layer thickness. Paulraj et al. [36] performed relevant research into the flow and heat transfer of several slot jets affecting different heat sources. Results proved that HTR decreases when the channel height increases. Boudraa et Bessaïh [37] investigated the behavior of fluid flow and heat transfer around a hot cubic block exposed to a cross-flow and an impinging jet. It was observed that changing the jet's location toward the channel inlet could enhance the HTR. Nimmagadda et al. [38] studied the effect of uniform/non-uniform magnetic field. It was found that increasing the strength of the magnetic field improves the HTR.

According to our knowledge of numerical and experimental researches conducted in this area, this is the first study relevant to turbulent forced convection analysis of water-Al₂O₃ nanofluid flow, heat transfer and entropy generation in a channel containing an array of heated blocks mounted on the bottom wall and influenced by the TPMM impinging jet. The main objective concerns the effects of various parameters such as Re, ϕ , D_b and the optimal position of J2 on the HTR. Some correlations of \overline{Nu} are obtained. This work can be improved thermal performance of some engineering industries.

2. Geometry description and mathematical model

The computational domain is a two-dimensional (2D) symmetric channel containing an array of heated blocks placed on the bottom wall and cooled by impinging jets (Figure 1). The geometric parameters are: $L = 0.04\text{m}$, $H = L$, $D_b = 3L/4$, $h = L/4$, $N = L/2$, $L1 = 16L$ where L, h are the length and height blocks, D_b is the space between each two blocks. The jets enter through the nozzle of width N, where the distance between it (nozzle) and the bottom wall is H.

Table 1. Physical properties of the water and Al₂O₃ at T= 293 K.

Properties	Water	Al ₂ O ₃
ρ	998.2	880
C_p	4182	36
μ	0.001003	3890
k	0.6	/



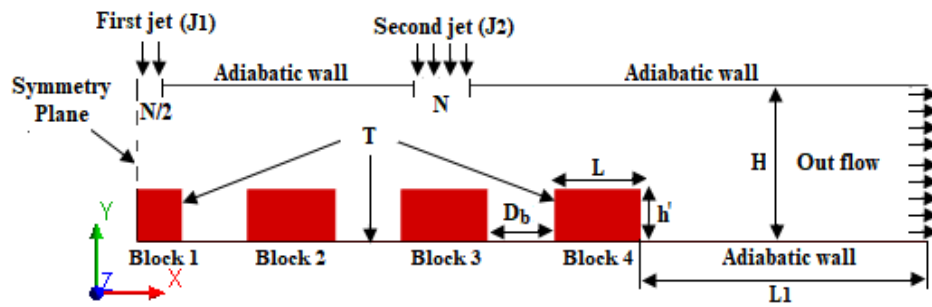


Fig. 1. Geometry.

The main properties of water and nanoparticles are given in Table 1 [17].

2.1 Assumptions

The heat transfer behavior of nanofluids is modeled using TPMM. Simplifying the study is made with the following assumptions:

- The flow is considered turbulent, incompressible and assumed to be a Newtonian fluid.
- The base fluid and nanoparticles to be in thermal equilibrium.
- The nanoparticles are assumed to be spherical shape, uniform in size and shape.
- The speed of the nanoparticles has the same speed as the base fluid.
- The dissipation of viscosity and approximation of Boussinesq are negligible.

2.2 Governing equations

Based on the assumptions mentioned above, the equations which govern the TPMM can be expressed as follows:

Continuity equation [39]:

$$\nabla \cdot (\rho_m \mathbf{V}_m) = 0 \quad (1)$$

Momentum equation [16]:

$$\nabla \cdot (\rho_m \mathbf{V}_m \mathbf{V}_m) = -\nabla P + \nabla \cdot (\nabla \mathbf{V}_m + \nabla \mathbf{V}_m^T) \mu_m + \nabla \cdot \sum_{k=1}^n (\rho_k \varphi_k \mathbf{V}_{dr,k} \mathbf{V}_{dr,k}) \quad (2)$$

Energy equation [41]:

$$\nabla \cdot \sum_{k=1}^n (\rho_k \varphi_k \mathbf{V}_k C_{p,k} T) = \nabla \cdot (\mathbf{K}_m \nabla T) \quad (3)$$

Volume fraction equation [42]:

$$\nabla \cdot (\varphi_{np} \rho_{np} \mathbf{V}_m) = -\nabla \cdot (\varphi_{np} \rho_{np} \mathbf{V}_{dr,np}) \quad (4)$$

The mixture velocity of nanofluid can be expressed as:

$$\mathbf{V}_m = \sum_{k=1}^n \frac{\varphi_k \rho_k \mathbf{V}_k}{\rho_m} \quad (5)$$

The drift velocity of the nanoparticle is:

$$\mathbf{V}_{dr,k} = \mathbf{V}_k - \mathbf{V}_m \quad (6)$$

The slip velocity is:

$$\mathbf{V}_{np,bf} = \mathbf{V}_{np} - \mathbf{V}_{bf} \quad (7)$$

The drift velocity and slip velocity can be related as:

$$\mathbf{V}_{dr,np} = \mathbf{V}_{np,bf} - \sum_{k=1}^n \frac{\varphi_k \rho_k \mathbf{V}_{fk}}{\rho_m} \quad (8)$$

Following equations proposed by [43] and [44], the slip velocity ($\mathbf{V}_{np,bf}$) and drag function (f_{drag}) are, respectively.

$$\mathbf{V}_{np,bf} = \frac{\rho_{np} d_p^2}{18 \mu_{bf} f_{drag}} \frac{(\rho_{np} - \rho_n)}{\rho_{np}} g - (\mathbf{V}_n \cdot \nabla) \mathbf{V}_m \quad (9)$$

$$f_{drag} = \begin{cases} 1 + 0.15 \text{Re}_p^{0.687}, & \text{Re}_p \leq 1000 \\ 0.0183 \text{Re}_p, & \text{Re}_p \geq 1000 \end{cases}, \quad \text{Re}_p = \frac{\mathbf{V}_m d_p}{\nu_m} \quad (10)$$



where V_m and d_p are the kinematics viscosity of mixture and nanoparticles diameter, respectively.

2.3 Turbulence model

For the standard $k-\varepsilon$ turbulence model, the turbulent kinetic energy (k) and the turbulent dissipation rate (ε) equations [45-46] are:

$$\nabla \cdot (\rho_m V_m k) = \left(\frac{\mu_{t,m}}{\sigma_k} \nabla k \right) + G_{k,m} - \rho_m \varepsilon \quad (11)$$

$$\nabla \cdot (\rho_m V_m \varepsilon) = \left(\frac{\mu_{t,m}}{\sigma_\varepsilon} \nabla \varepsilon \right) + \frac{\varepsilon}{k} (C_1 G_{k,m} - C_2 \rho_m \varepsilon) \quad (12)$$

where $\mu_{t,m}$ and $G_{k,m}$ are given as follows:

$$\mu_{t,m} = \rho_m C_\mu \frac{k^2}{\varepsilon} \quad (13)$$

$$G_{k,m} = \mu_{t,m} (\nabla V_m + (\nabla V_m)^T) \quad (14)$$

$C_1, C_2, C_\mu, \sigma_k$ and σ_ε are empirical constants: $C_1 = 1.44, C_2 = 1.92, C_\mu = 0.09, \sigma_k = 1.0$ and $\sigma_\varepsilon = 1.3$.

The nanofluid properties are calculated as:

- Density [47]:

$$\rho_m = (1 - \varphi) \rho_{bf} + \varphi \rho_{np} \quad (15)$$

- Specific heat [48]:

$$C_{p,m} = \frac{(1 - \varphi) C_{p,bf} \rho_{bf} + \varphi C_{p,np} \rho_{np}}{\rho_m} \quad (16)$$

- Dynamic viscosity [49]:

$$\mu_m = (1 + 7.3\varphi + 123\varphi^2) \mu_{bf} \quad (17)$$

- Thermal conductivity [50]:

$$k_m = k_{bf} \left[\frac{k_{np} + 2k_{bf} + 2\varphi(k_{np} - k_{bf})}{k + 2k_{bf} - 2\varphi(k_{np} - k_{bf})} \right] \quad (18)$$

The total entropy generation includes the fluid friction and heat transfer terms are defined as [51]:

$$\dot{S} = \dot{S}_{g,th} - \dot{S}_{g,v} \quad (19)$$

$$\dot{S}_{g,th} = \frac{k_m}{T^2} \left(\left(\frac{\partial T}{\partial x} \right)^2 + \left(\frac{\partial T}{\partial y} \right)^2 \right) \quad (20)$$

$$\dot{S}_{g,v} = \frac{\mu_m}{T} \left(2 \left[\left(\frac{\partial u}{\partial x} \right)^2 + \left(\frac{\partial v}{\partial y} \right)^2 \right] + \left[\left(\frac{\partial u}{\partial y} \right) + \left(\frac{\partial v}{\partial x} \right) \right]^2 \right) \quad (21)$$

Table 2. Boundary conditions.

Type	U_i (m / s)	V_i (m / s)	T (K)
First jet inlet (J1)	0	v_j	293
Second jet inlet (J2)	0	v_j	293
Outflow	$\frac{\partial u}{\partial x} = 0$	$\frac{\partial v}{\partial x} = 0$	$\frac{\partial T}{\partial x} = 0$
Symmetric side	0	$\frac{\partial v}{\partial x} = 0$	$\frac{\partial T}{\partial x} = 0$
wall	0	0	$\frac{\partial T}{\partial x} = \frac{\partial T}{\partial y} = 0$
Temperature	0	0	343



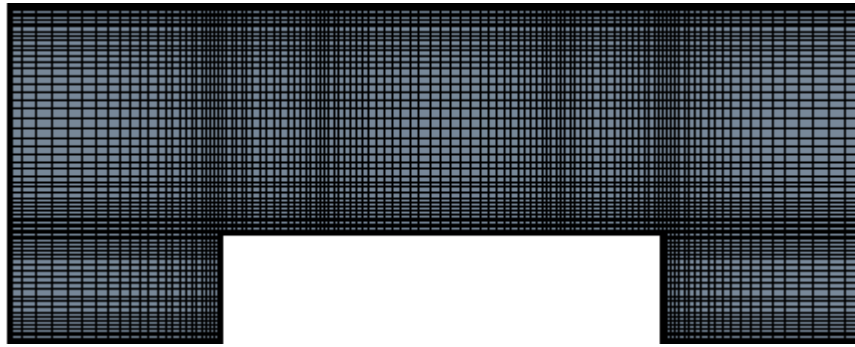
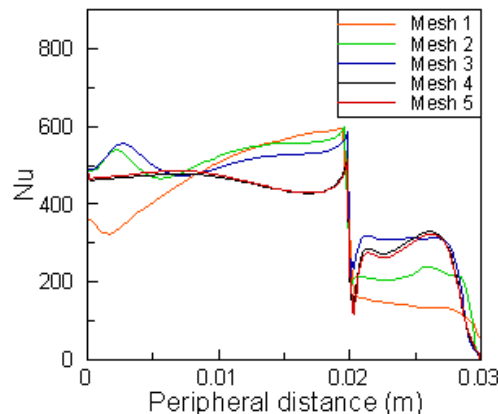


Fig. 2. Computational grid.

Fig. 3. Variation of local Nu for the first block with different tested grids at $\varphi = 5\%$ and $Re = 20000$.

2.4 Boundary conditions

The boundary conditions used are summarized in Table 4. At the jets inlet (J1 and J2), it was assumed that the flow is turbulent at a uniform velocity (V_j). At the channel exit, all gradients are equal to zero, the upper and bottom wall except for the hot part are adiabatic with nonslip condition, the distance around the blocks and between them are assumed under constant temperature with nonslip condition. At the symmetric side, we assumed that zero normal gradients of all variables.

3. Computational model

The Ansys-Fluent 14.5 software [52] was used for simulating the turbulent heat transfer flow. We have used second upwind order scheme and the SIMPLE algorithm. In order to confirm the negligible effect of the grid on the results performed by raising the mesh density successively until further refinement revealed a difference between the consecutive results of less than 1% and according to the best compromise between precision and available calculation means, a grid of approximately 110.000 structured quadrilateral cells (1100 x 100 in the x and y directions, respectively) was adopted for all cases we studied as shown in Figure 2. This mesh was designed to capture the sharp gradients and boundary layers near the wall and the blocks.

3.1 Grid independence study

The mesh independence test was performed for Al₂O₃–water nanofluid with $Re = 20000$ and $\varphi = 5\%$. Figure 2 shows the distribution of Nu along the first heated block calculated on five (5) different meshes (see table 3). After comparing the five cases, the mesh number 4 was chosen as an acceptable mesh.

4. Results and discussion

A numerical analysis related to the turbulent forced convection of water-Al₂O₃ nanofluid is carried out to analyze the fluid flow, heat transfer and entropy generation in a channel containing heated blocks, mounted on the bottom wall and cooled by impinging jets. The parameters are Re , φ , D_b and the position optimal of the J2. We present Nu , \overline{Nu} , $\dot{S}_{g,th}$, \overline{Cf} , $\dot{S}_{g,t}$ and Be . Various correlations for \overline{Nu} are presented.

Table 3. Number of nodes for various meshes.

Mesher	1	2	3	4	5
Number of nodes	715x70	875x80	1000x90	1000x100	1217x115



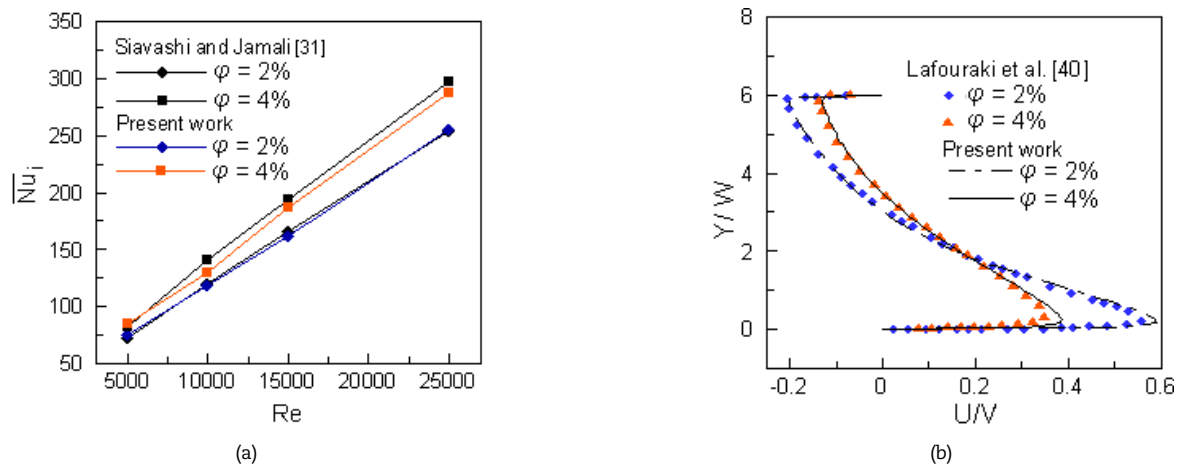


Fig. 4. Comparison of present research with data available.

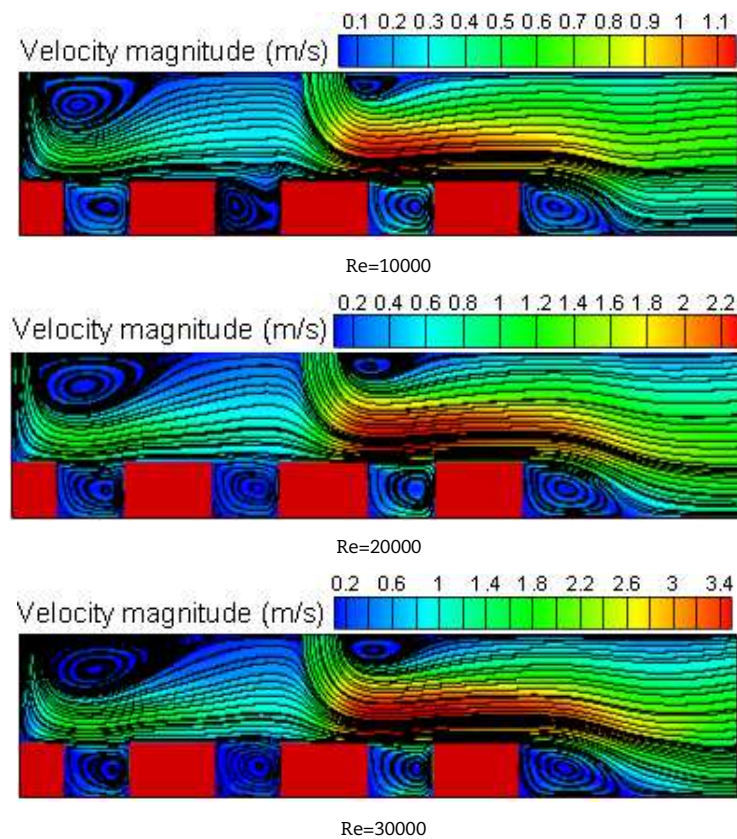


Fig. 5. Effect of Re on stream function and velocities magnitude contours for different Re at $\phi = 5\%$.

4.1 Validation

In order to confirm the validity of the fluid flow and heat transfer solution, we used the standard $k-\epsilon$ turbulence model with enhanced wall treatment by employing TPM. Our results are compared with [31] and [40], and are shown in Figure 4a and Figure 4b, respectively. The first figure (4a) shows a good agreement with the work of Siavashi and Jamali [31] by comparing the \overline{Nu} at different Re ($Re = 5000$ to 25000). With regard to the second figure (4b), a similar trend is observed with the results of Lafouraki et al. [40], based on the comparison of the velocity magnitude at $\phi = 2\%$ and $\phi = 4\%$.

4.2 Effect of Reynolds number

Figure 5 represents the streamline and magnitude velocity contours one on the other at different Re ($Re = 10000, 20000$ and 30000) using Al₂O₃-water nanofluid with $\phi = 5\%$. It can be noted that the size of the vortex formed at neighborhood jets increases with Re , where the J1 is located in the middle of the upper surface of the symmetric channel and J2 located on the middle of the third block. The increase in Re results in an increase of the intensity of the vortices formed in the channel between the heated blocks, after the last block the recirculation zone formed due to sudden expansion, this vortex also increases with Re . A higher streamline concentration (where speed takes great values) was found at the top of the blocks 3 and 4 due to the dominance of the J2.



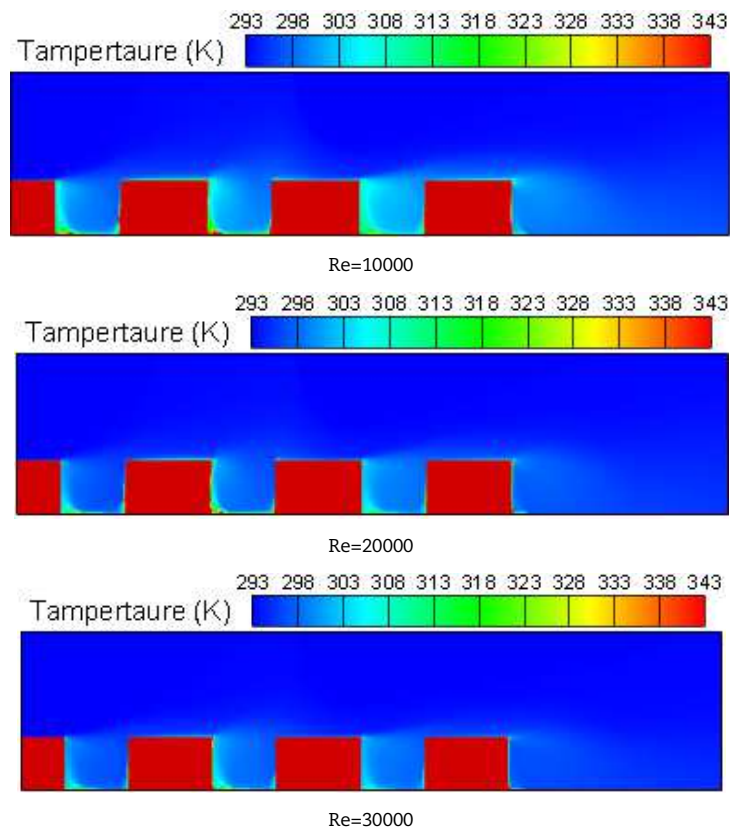


Fig. 6. Effect of Re on isothermal contours, at $\varphi = 5\%$.

Figure 6 presents the effect of Re (Re=10000, 20000 and 30000) on the temperature distribution around the heated blocks, at $\varphi = 5\%$. We can observe that the isotherms occupy a considerable part of channel around and between the heated block for a low Re (Re=10000), because of that momentum of nanofluid not enough to decrement thermal layer. Note the opposite when increasing Re. This means that the thermal boundary layer thickness gradually decreases when Re increases.

Figure 7 illustrates the distribution of Nu in terms of Re around four (4) heated blocks, at $\varphi = 5\%$. Results show that an increase in Re allows an increase in Nu at the top of each block due to a reduction in thermal boundary layer thickness. Figure 7 (a-d) shows the increase of Nu on the left and right sides of the blocks with the increase of Re. This is due to the increase in the intensity of the vortices that form between each block in the channel. We observe that the Nu distribution around block 2 is the same as block 4 with a difference in values of Nu. The maximum values of Nu are located around the last block due to deflection of the J2 and the domination of this jet (J2) compared to J1.

Figure 8 depicts the variation of \overline{Nu} and \overline{Cf} around each heated block, at $\varphi = 5\%$ and different Re. It can be noted that the increase in Re is accompanied by an increase \overline{Nu} and a reduction in \overline{Cf} . Decrease in \overline{Cf} at high Re is due to decreases in boundary layer thickness, so the velocity and temperature gradients increase. This leads to increase in \overline{Cf} . This means that the HTR is improved.

4.3 Effect of volume fraction

Figure 9 shows the variation of average \overline{Nu} around of each heated block with different φ , at Re=20000. We can observe that all nanofluids have higher \overline{Nu} than those of the pure water ($\varphi = 0$), because as we know the increase in φ improves thermophysical properties of the Al_2O_3 -water nanofluid. Also, we can note that the \overline{Nu} increases with increasing φ , because of the large exchange of energy due to the chaotic motion of nanoparticles, hence HTR is enhanced with increase in φ . We can conclude that the maximum values of \overline{Nu} , located around the last block, is due the domination of the J2 compared to J1.

4.4 Effect of the second jet position

To choose the optimal position of J2 to improve the HTR, we changed the position of J2 several times (see Table 4.) along the upper wall. Figure 10 illustrates the variation of \overline{Nu} for different positions of the J2, at $\varphi = 3\%$ and different Re. We can note that HTR increases with increasing in Re due to the increase of the length and strength of the recirculation zones formed between the heated blocks, which allows decreasing the thermal boundary layer thickness, so HTR is improved. Changing the position of the J2 towards the J1 also enhances HTR. This allows us to take advantage of the lost momentum of the J2, which increases the temperature and velocity gradients along the heated blocks. We can conclude that the optimal location for the J2, which gives the highest HTR is located on the second block.



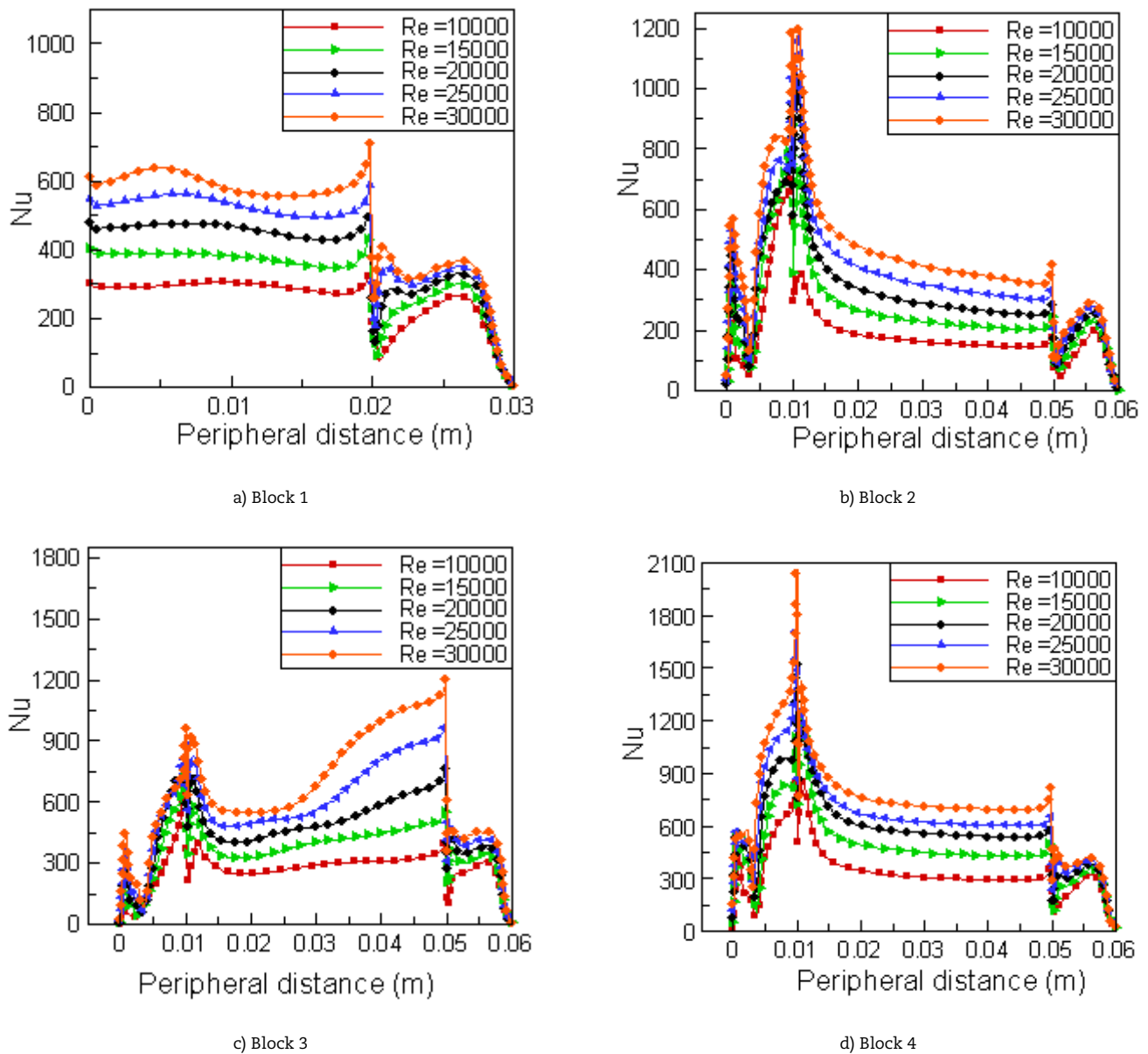


Fig. 7. Variation of Nu with peripheral distance and Re for different blocks, at $\varphi = 5\%$.

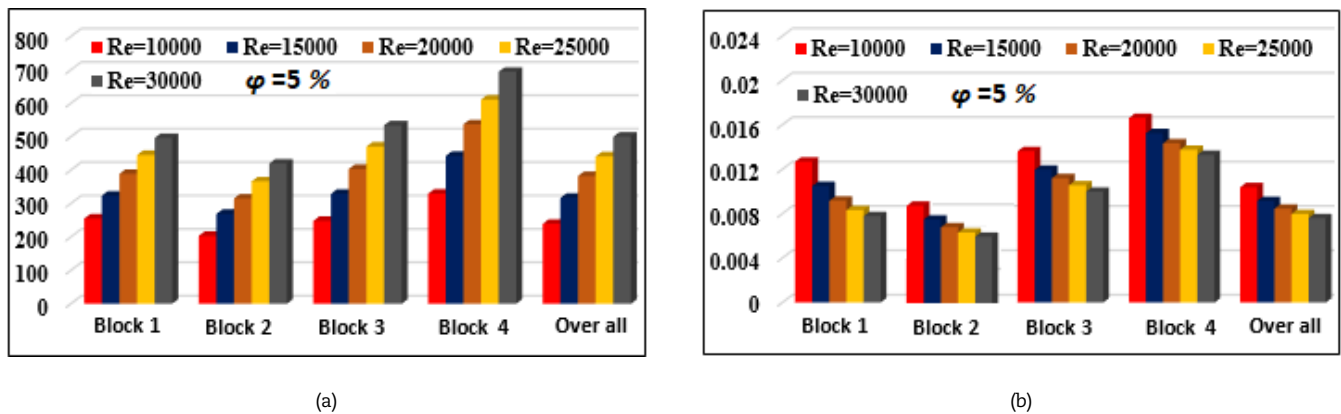


Fig. 8. a) Variation of \overline{Nu} around the exposed surface of different heated blocks for various Re, at $\varphi = 5\%$

b) Variation of \overline{Cf} around the exposed surface of different heated blocks for various Re, at $\varphi = 5\%$



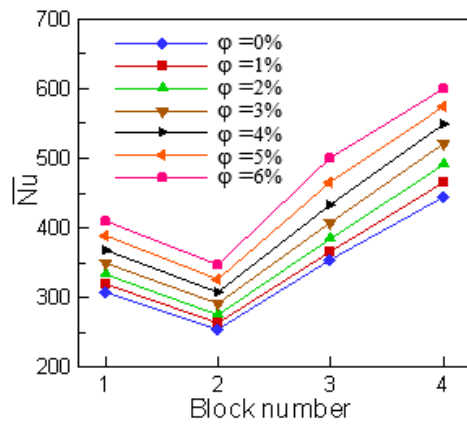


Fig. 9. Variation of \overline{Nu} around the exposed surface of different heated blocks for various φ , at $Re=20000$.

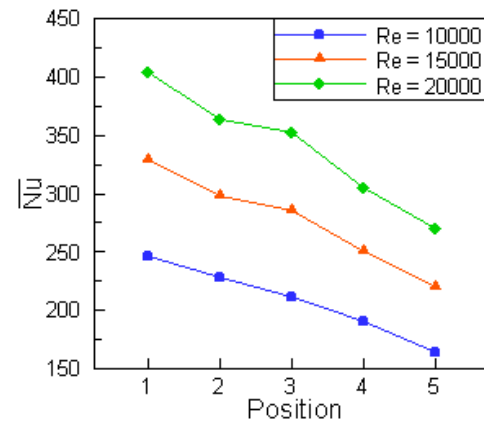


Fig. 10. Variation of \overline{Nu} along the heated blocks for different position of J2 at $\varphi = 3\%$ and different Re.

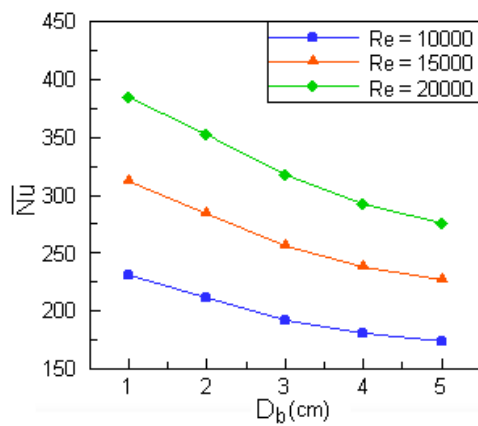


Fig. 11. Variation of \overline{Nu} along the heated blocks for different D_b , at $\varphi = 5\%$ and different Re.

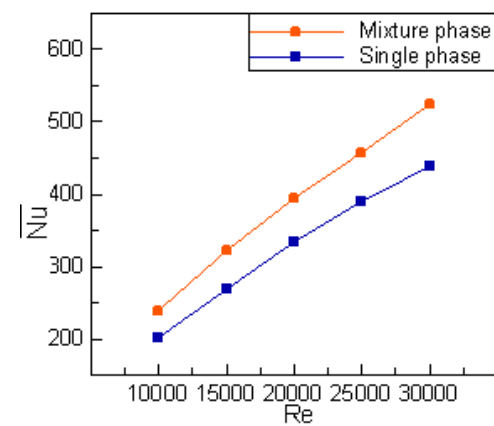
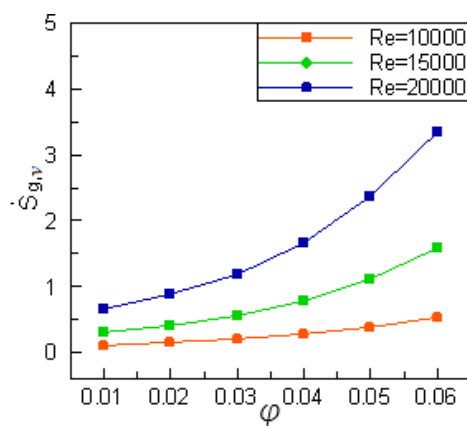
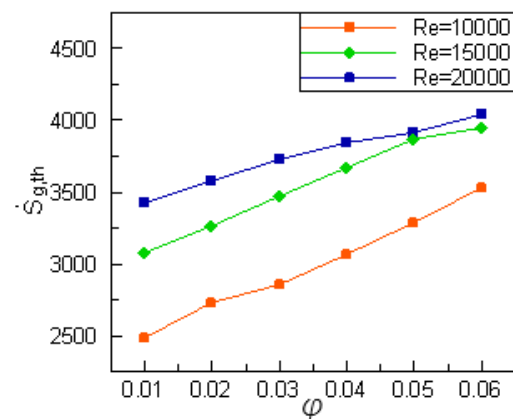


Fig. 12. Comparison of \overline{Nu} for different heated blocks between mixture and single phase model, at different Re and $\varphi = 5\%$.



(a)



(b)

Fig. 13. The effect of φ on a) $\dot{S}_{g,th}$ and b) $\dot{S}_{g,v}$

Table 4. Different distances between J1 and J2.

Position	1	2	3	4	5
Distance between J1 and J2 (cm)	7.5	11.5	14	17.5	21



4.5 Effect of spacing between heated blocks

Figure 11 depicts the effect of D_b on \overline{Nu} of Al₂O₃–water nanofluid, at $\varphi = 5\%$ with different Re. The position of the second jet is fixed on the third block despite the change of D_b . We found that the increase in Re contributes significantly to the improvement in the HTR. So the influence of the jets on the heated blocks leads to increases the temperature and velocity gradients, when we increase in D_b we get the opposite, which means the HTR decreases.

4.6 Comparison between single and two-phase model

Figure 12 presents the comparison of the \overline{Nu} for different Re at $\varphi = 5\%$ with both SPM and TPMM. According to these results, we can observe that the values of \overline{Nu} increase with the increase of Re, where the values of \overline{Nu} in the TPMM model are higher than the SPM, the same results were found by [14, 53].

4.7 Entropy generation analysis

Figure 13 illustrates the φ effect on $\dot{S}_{g,th}$ and $\dot{S}_{g,v}$ at different Re. Results revealed that the $\dot{S}_{g,th}$ and $\dot{S}_{g,v}$ values increase with the increase of φ due the improvement of thermal conductivity and viscosity of fluid by adding nanoparticles. The values of both $\dot{S}_{g,th}$ and $\dot{S}_{g,v}$ are also increasing due the increased in velocity and temperature gradients with the increase in Re. So, $\dot{S}_{g,th}$ and $\dot{S}_{g,v}$ increasing with the increase in φ and Re.

Figure 14a illustrates the φ effect on $\dot{S}_{g,t}$ at different Re. Results show that the values of $\dot{S}_{g,t}$ increase with the increase in Re and φ , with regard to Figure 11b, which illustrates the φ effect on Be at different Re. The increase in φ and Re leads to reduce the values of Be, this decreases is due to the increase in $\dot{S}_{g,v}$ and $\dot{S}_{g,th}$ with Re and φ (See Fig. 11a and Fig. 11b). From Figures 11a and 10b, and by using the definition of Be ($Be = \dot{S}_{g,th} / \dot{S}_{g,t}$), we can explain that lower values obtained by saying that the $\dot{S}_{g,th}$ values are much greater than $\dot{S}_{g,v}$ ($\dot{S}_{g,th}$ dominate on $\dot{S}_{g,v}$). In [54], the same results were obtained.

Figure 15 shows the variation of $\dot{S}_{g,t}$ for different position of J2, at $\varphi = 3\%$ with different Re. We can note that $\dot{S}_{g,t}$ increases with increasing in Re due the increased in velocity and temperature gradients with the increase in the values of Re. Also, we can clearly notice that by changing the position of the second towards the first jet, this allows us to take advantage of the lost momentum of the J2, which increases the temperature and velocity gradients along the heated blocks. So the $\dot{S}_{g,t}$ increases and takes its highest values over the second block.

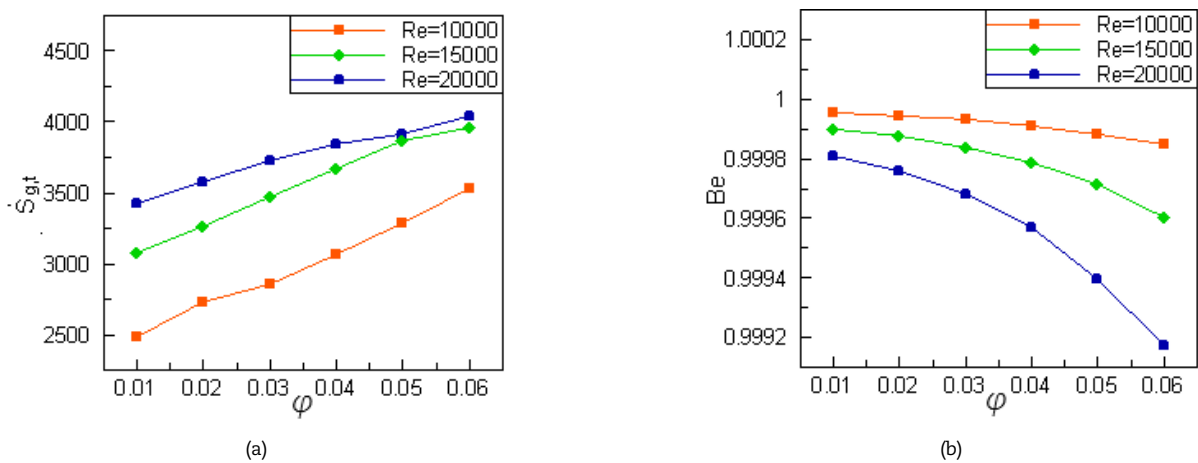


Fig. 14. The effect of φ on a) $\dot{S}_{g,t}$ and b) Be

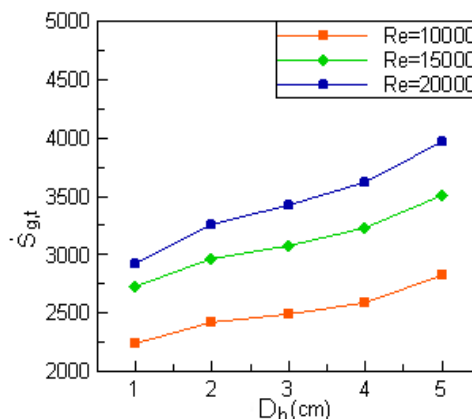
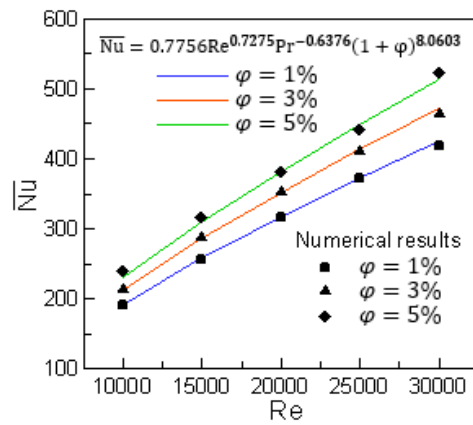
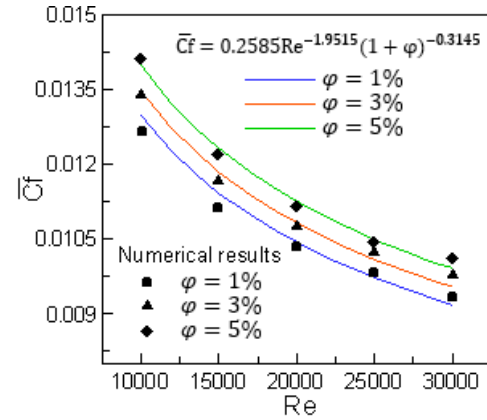
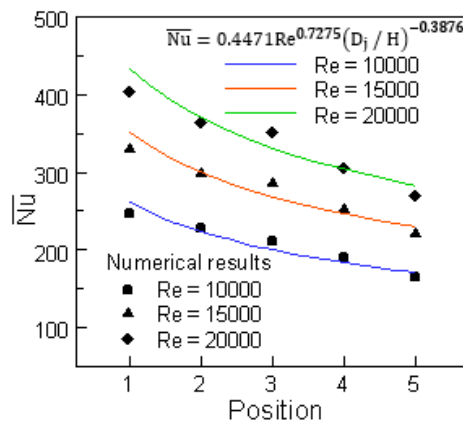
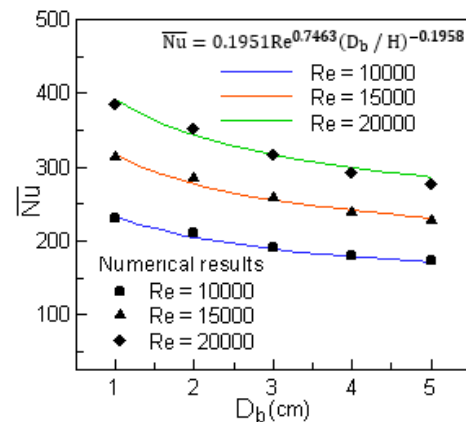


Fig. 15. The effect of D_b on $\dot{S}_{g,t}$.



Fig. 16. Correlation of \overline{Nu} for different Re and φ .Fig. 17. Correlation of \overline{Cf} for different Re and φ .Fig. 18. Correlation of the \overline{Nu} for different Re and D_j .Fig. 19. Correlation of \overline{Nu} for different Re and D_b .

4.8 Correlations

The first correlation proposed is related of the \overline{Nu} along the heated blocks, presented as follows:

$$\overline{Nu} = 0.7756 Re^{0.7275} Pr^{-0.6376} (1 + \varphi)^{8.0603} \quad (22)$$

and it is validated with the numerical results for an error between -1.5% and 3.5%, as shown in Figure 16. This correlation is defined as function of the Re, Pr and φ ($cRe^n Pr^m (1 + \varphi)^t$), where $10000 \leq Re \leq 30000$ and $1\% \leq \varphi \leq 5\%$. In addition, this correlation can help engineers working in the industry who need to design this configuration.

The second correlation that we proposed relates to \overline{Cf} along the heated blocks, presented as follows:

$$\overline{Cf} = 0.2585 Re^{-1.9515} (1 + \varphi)^{-0.3145} \quad (23)$$

and it is available with the numerical results for an error not exceeding 3%, as shown in Figure 17. This correlation is defined as function of the Re and φ ($cRe^n (1 + \varphi)^t$), where $10000 \leq Re \leq 30000$ and $1\% \leq \varphi \leq 5\%$.

The third correlation proposed for the calculation of \overline{Nu} along the heated blocks for different spaces between jets D_j is presented as follows:

$$\overline{Nu} = 0.4471 Re^{0.7275} (D_j/H)^{-0.3876} \quad (24)$$

and it is validated for an error 3% as shown in Figure 18. This correlation is defined as function of the Re and D_j/H ($cRe^n (D_j/H)^t$), where $10000 \leq Re \leq 30000$ and $\varphi = 5\%$.

The last correlation proposed for the calculation of \overline{Nu} along the heated blocks for different spaces between blocks (D_b) is presented as follows:

$$\overline{Nu} = 0.1951 Re^{0.7463} (D_b/H)^{-0.1958} \quad (25)$$

and it is validated with the numerical results for an error between -1.5% and 3.5%, as shown in Figure 19. This correlation is defined as function of the Re and D_b/H ($cRe^n (D_b/H)^t$), where $10000 \leq Re \leq 30000$ and $1\text{cm} \leq D_b \leq 5\text{cm}$ for $\varphi = 1\%$.



5. Conclusion

A numerical study revealed the influence of different parameters on the behavior of water- Al₂O₃ nanofluid flow, heat transfer and entropy generation in a symmetrical channel containing heated blocks and cooled by impinging jets. The most important results obtained in the study that we conducted are:

- The increase of Re and φ improves the HTR.
- The decrease of D_b can significantly contribute to increasing the HTR.
- The increase in Re and change the located of the J2 towards the J1 enhanced the HTR, and we got the highest values of HTR when we fixed the position of J2 on the second block.
- The maximum values of \overline{Nu} , located around the last block, is due the domination of the J2 compared to J1.
- TPMM gives higher \overline{Nu} values than the SPM.
- Different correlations are proposed for \overline{Nu} .
- The increase in values of Re and φ leads to increase of $\dot{S}_{g,v}$, $\dot{S}_{g,th}$ and $\dot{S}_{g,t}$.
- Be is approximately equal to 1 at the cases, because of the dominance of $\dot{S}_{g,th}$.
- The increase in Re and D_b values increases $\dot{S}_{g,t}$.
- The increase in Re and the change of the located J2 towards the J1 increases the values of $\dot{S}_{g,t}$.

Our future perspective based on studying effect of the nanoparticles shape using hybrid nanofluid with different models of turbulence such as SST kw, RSM..., study the effect of some parameters geometric on the HTR such as length and height of hot blocks, we reformulate the current study using more complex 3D geometries.

Author Contributions

The manuscript was written through the contribution of all authors. All authors discussed the results, reviewed, and approved the final version of the manuscript.

Acknowledgments

The authors are thankful to the anonymous reviews and editor for the valuable comments that helped to improve the quality of the presented work.

Funding

This research did not receive any specific grant from funding agencies in the public, commercial, or not-for-profit sectors.

Conflict of Interest

The authors declared no potential conflicts of interest with respect to the research, authorship, and publication of this article.

Nomenclature

Be	Bejan number	$\dot{S}_{g,t}$	Total entropy generation (W/m ³ k)
\overline{Cf}	Friction factor	$\dot{S}_{g,th}$	Thermal entropy generation (W/m ³ k)
C_p	Specific heat (J/kgk)	$\dot{S}_{g,v}$	Frictional entropy generation (W/m ³ k)
d_p	Nanoparticles diameter (m)	T	Temperature (K)
D_b	Spacing between blocks (m)		

Abbreviations

HTR	Heat transfer rate
SPM	Single phase model
SPMM	Single phase mixture model
TPMM	Two phase mixture model

Greek symbols

φ	Volume fraction of nanoparticles (%)
ρ	Density (kg/m ³)
μ	Dynamic viscosity (kg/ms)
ν	Kinematics viscosity (m ² /s)

Subscripts

bf	base fluid
m	mixture

D_j	Distance between J1 and J2
f_{drag}	Drag function
g	Gravitational acceleration (m/s ²)
\bar{h}	Heat transfer coefficient (W/m ² k)
h'	Height block (m)
H	Channel height (m)
k	Thermal conductivity (W/mk)
L	Length blocks (m)
N	Width of the jets inlet (m)
Nu	Nusselt number
\overline{Nu}	Average Nusselt number
P	Pressure (Pa)



Pr	Prandtl number	np	nanoparticle
Re	Reynolds number	dr,k	drift of water or nanoparticle


References


- [1] Menni, Y., Ghazvini, M., Ameer, H., Hossein, Ahmadi, M., Sharifpur, M., Sadeghzadeh, M., Numerical calculations of the thermal aerodynamic characteristics in a solar duct with multiple V-baffles, *Engineering Applications of Computational Fluid Mechanics*, 14(1), 2020, 1173–1197.
- [2] Menni, Y., Ghazvini, M., Ameer, H., Kim, M., Ahmadi, M.H., Sharifpur, M., Combination of baffling technique and high-thermal conductivity fluids to enhance the overall performances of solar channels, *Engineering with Computers*, 2020, <https://doi.org/10.1007/s00366-020-01165-x>.
- [3] Menni, Y., Chamkha, A.J., Azzi, A., Fluid Flow and Heat Transfer over Staggered '+' Shaped Obstacles, *Journal of Applied and Computational Mechanics*, 6(4), 2020, 741–756.
- [4] Menni, Y., Azzi, A., Chamkha, A., Enhancement of convective heat transfer in smooth air channels with wall-mounted obstacles in the flow path, *Journal of Thermal Analysis and Calorimetry*, 135, 2019, 1951–1976.
- [5] Sobamowo, M.G., Free Convection Flow and Heat Transfer of Nanofluids of Different Shapes of Nano-Sized Particles over a Vertical Plate at Low and High Prandtl Numbers, *Journal of Applied and Computational Mechanics*, 5(1), 2020, 13–39.
- [6] Hamzah, H.K., Ali, F.H., M., Hatami, Jing, D., Effect of Two Baffles on MHD Natural Convection in U-Shape Superposed by Solid Nanoparticle having Different Shapes, *Journal of Applied and Computational Mechanics*, 6(SI), 2020, 1200–1209.
- [7] Paulraj, M.P., Byon, C., Vallati, A., Parthasarathy, R.K., A Numerical Investigation of Flow and Heat Transfer of Laminar Multiple Slot Jets Impinging on Multiple Protruding Heat Sources, *Heat Transfer Engineering*, 2018, 1–53.
- [8] Menni, Y., Chamkha, A.J., Massarotti, N., Ameer, H., Kaid, N., Bensafi, M., Hydrodynamic and thermal analysis of water, ethylene glycol and water-ethylene glycol as base fluids dispersed by aluminum oxide nano-sized solid particles, *International Journal of Numerical Methods for Heat and Fluid Flow*, 30(9), 2019, 4349–4386.
- [9] Rahim, K.A., Ahmed, M.A., Numerical investigation on the heat transfer enhancement using a confined slot impinging jet with nanofluid, *Propulsion and Power Research*, 8(4), 2019, 351–361.
- [10] Menni, Y., Chamkha, A.J., Zidani, C., Benyoucef, B., Numerical analysis of heat and nanofluid mass transfer in a channel with detached and attached baffle plates, *International Journal of Numerical Methods for Heat and Fluid Flow*, 6(1), 2019, 52–60.
- [11] Menni, Y., Chamkha, A.J., Zidani, C., Benyoucef, B., Heat and nanofluid transfer in baffled channels of different outlet models, *Mathematical Modeling of Engineering Problems*, 6(1), 2019, 21–28.
- [12] Menni, Y., Chamkha, A.J., Ahmed, A., Nanofluid flow in complex geometries - a review, *Journal of Nanofluids*, 8(5), 2018, 893–916.
- [13] Younes, M., Ahmed, A., Ali J. C., Nanofluid Transport in Porous Media: A Review, *Special Topics & Reviews in Porous Media, An International Journal*, 9(4), 2018, 1–16.
- [14] Abdelrehim, O., Khater, A., Mohamad, A.A., Radwan, A., Two-phase simulation of nanofluid in a confined single impinging jet, *Case Studies in Thermal Engineering*, 14, 2019, 100423.
- [15] Sheikholeslami, M., Abohamzeh, E., Jafaryar, M., Shafee, A., Babazadeh, H., CuO nanomaterial two-phase simulation within a tube with enhanced turbulator, *Powder Technology*, 373, 2020, 1–13.
- [16] Sheikholeslami, E., Jafaryar, M., Abohamzeh, M., Shafee, A., Babazadeh, H., Energy and entropy evaluation and two-phase simulation of nanoparticles within a solar unit with impose of new turbulator, *Sustainable Energy Technologies and Assessments*, 39, 2020, 100727.
- [17] Selimefendigil, F., Öztop, H.F., Pulsating nanofluids jet impingement cooling of a heated horizontal surface, *International Journal of Heat and Mass Transfer*, 69, 2014, 54–65.
- [18] Selimefendigil, F., Öztop, H.F., Analysis and predictive modeling of nanofluid-jet impingement cooling of an isothermal surface under the influence of a rotating cylinder, *International Journal of Heat and Mass Transfer*, 121, 2018, 233–245.
- [19] Izadi, A., Siavashi, M., Xiong, Q., Impingement jet hydrogen, air and CuH₂O nanofluid cooling of a hot surface covered by porous media with non-uniform input jet velocity, *International Journal of Hydrogen Energy*, 44, 2019, 15933–15948.
- [20] Lamraoui, H., Mansouri, K., Saci, R., Numerical investigation on fluid dynamic and thermal behavior of a non-Newtonian Al₂O₃-water nanofluid flow in a confined impinging slot jet, *Journal of Non-Newtonian Fluid Mechanics*, 265, 2019, 11–27.
- [21] Manca, O., Ricci, D., Nardini, S., Lorenzo, G.D., Thermal and fluid dynamic behaviors of confined laminar impinging slot jets with nanofluids, *International Communications in Heat and Mass Transfer*, 70, 2016, 15–26.
- [22] Amjadian, M., Safarzadeh, H., Bahraei, M., Nazari, S., Jaber, B., Heat transfer characteristics of impinging jet on a hot surface with constant heat flux using Cu₂O–water nanofluid: An experimental study, *International Communications in Heat and Mass Transfer*, 112, 2020, 104509.
- [23] Yousefi, T., Shojaeizadeh, E., Mirbagheri, H.R., Farahbaksh, B., Saghir, M.Z., An experimental investigation on the impingement of a planar jet of Al₂O₃-water nanofluid on a V-shaped plate, *Experimental Thermal and Fluid Science*, 50, 2013, 114–126.
- [24] Teamah, M.A., Dawood, M.M.K., Shehata, A., Numerical and experimental investigation of flow structure and behavior of nanofluids flow impingement on horizontal flat plate, *Experimental Thermal and Fluid Science*, 74, 2016, 235–246.
- [25] Mahdavi, M., Sharifpur, M., Meyer, J.P., Chen, L., Thermal analysis of a nanofluid free jet impingement on a rotating disk using volume of fluid in combination with discrete modelling, *International Journal of Thermal Sciences*, 158, 2020, 106532.
- [26] Sun, B., Qu, Y., Yang, D., Heat transfer of Single Impinging Jet with Cu Nanofluids, *Applied Thermal Engineering*, 102, 2016, 701–707.
- [27] Pratap, A., Kumar, Baghel, Y., Patel, V.K., Effect of impingement height on the enhancement of heat transfer with circular confined jet impingement using nanofluids, *Materials Today: Proceedings*, 28, 2020, 1656–1661.
- [28] Abhijith, M.S., Venkatasubbiah, K., Numerical investigation of jet impingement flows with different nanofluids in a mini channel using Eulerian-Eulerian two-phase method, *Thermal Science and Engineering Progress*, 2020, 100585.
- [29] Abanti, D., Sonal, K., Pabitra, H., Heat Transfer and Thermal Characteristics Effects on Moving Plate Impinging from Cu-Water Nanofluid Jet, *Journal of Thermal Science*, 29(1), 2020, 182–193.
- [30] Esbo, M.R., Ranjbar, A.A., Ramiar, A., Rahgoshay, M., Numerical simulation of forced convection of nanofluid in a confined jet, *Heat & Mass Transfer*, 48, 2012, 1995–2005.
- [31] Siavashi, M., Jamali, M., Heat transfer and entropy generation analysis of turbulent flow of TiO₂-water nanofluid inside annuli with different ratios using two-phase mixture model, *Applied Thermal Engineering*, 100, 2016, 1149–1160.
- [32] Lafouraki, B.Y., Ramiar, A., Ranjbar, L.A., Numerical Investigation of Laminar Forced Convection and Entropy Generation of Nanofluid in a Confined Impinging Slot Jet Using Two Phase Mixture Model, *J. Sci. Technol. Trans. Mech. Eng.*, 43, 2019, 165–179.
- [33] Paulraj, M.P., Sahu, S.K., Conjugate heat transfer enhancement of laminar slot jets with various nanofluids on an array of protruding hot sources using MPM approach, *Numerical Heat Transfer*, 76(4), 2019, 232–253.
- [34] Arquis, E., Rady, M.A., Nada, S.A., A numerical investigation and parametric study of cooling an array of multiple protruding heat sources by a laminar slot air jet, *International Journal of Heat and Fluid Flow*, 28, 2007, 787–805.
- [35] Lam, P.A.K., Prakash, K.A., A numerical investigation of heat transfer and entropy generation during jet impingement cooling of protruding heat sources without and with porous medium, *Energy Conversion and Management*, 89, 2015, 626–643.
- [36] Lam, P.A.K., Prakash, K.A., Thermodynamic investigation and multi-objective optimization for jet impingement cooling system with Al₂O₃/water nanofluid, *Energy Conversion and Management*, 111, 2016, 38–56.
- [37] Boudraa, B., Bessaih, R., Three-dimensional turbulent forced convection around a hot cubic block exposed to across-flow and an impinging jet, *Heat Transfer*, 2020, 1–19.
- [38] Nimmagadda, R., Haustein, H.D., Asirvatham, L.G., Wongwises, S., Effect of uniform/non-uniform magnetic field and jet impingement on the hydrodynamic and heat transfer performance of nanofluids, *Journal of Magnetism and Magnetic Materials*, 479, 2019, 268–281.
- [39] Ghale, Z.Y., Haghshenasfard, M., Esfahany, M.N., Investigation of nanofluids heat transfer in a ribbed microchannel heat sink using single-phase and multiphase CFD models, *International Communications in Heat and Mass Transfer*, 68, 2015, 122–129.
- [40] Lafouraki, B.Y., Ramiar, A., Ranjbar, L.A., Numerical Simulation of Two Phase Turbulent Flow of Nanofluids in Confined Slot Impinging Jet, *Flow Turbulence Combust*, 97, 2016, 571–589.



- [41] Shariat, M., Moghari, R.M., Akbarinia A., Rafee, R., Sajjadi S.M., Impact of nanoparticle mean diameter and the buoyancy force on laminar mixed convection nanofluid flow in an elliptic duct employing two phase mixture model, *International Communications in Heat and Mass Transfer*, 50, 2014, 15-24.
- [42] Hejazian, M., Moraveji, M.K., Beheshti, A., Comparative study of Euler and mixture models for turbulent flow of Al₂O₃ nanofluid inside a horizontal tube, *International Communications in Heat and Mass Transfer*, 52, 2014, 152-158.
- [43] Manninen, M., Taivassalo, V., Kallio, S., *On the mixture model for multiphase flow*, VTT Publications 288 Technical Research Centre of Finland, 1996.
- [44] Schiller, L., Naumann, A., A drag coefficient correlation, *Z. Ver. Dtsch Ing.*, 7, 1935, 318-320.
- [45] Bazdar, H., Toghraie, D., Pourfattah, F., Akbari, O.A., Nguyen H.M., Asadi, A., Numerical investigation of turbulent flow and heat transfer of nanofluid inside a wavy microchannel with different wavelengths, *Journal of Thermal Analysis and Calorimetry*, 139, 2020, 2365-2380.
- [46] Esmaeili, H., Armaghani, T., Abedini, A., Pop, I., Turbulent combined forced and natural convection of nanofluid in a 3D rectangular channel using two-phase model approach, *Journal of Thermal Analysis and Calorimetry*, 135, 2019, 3247-3257.
- [47] Shahsavari, A., Rashidi, M., Mosghani, M.M., Toghraie, D., Talebizadehsardari, P., A numerical investigation on the influence of nano additive shape on the natural convection and entropy generation inside a rectangle shaped finned concentric annulus filled with boehmite alumina nanofluid using two phase mixture model, *Journal of Thermal Analysis and Calorimetry*, 141, 2020, 915-930.
- [48] Alsabery, A.I., Ismael, M.A., Chamkha, A.J., Hashim, I., Effects of two-phase nanofluid model on MHD mixed convection in a lid-driven cavity in the presence of conductive inner block and corner heater, *Journal of Thermal Analysis and Calorimetry*, 135, 2019, 729-750.
- [49] Ghale, Z.Y., Haghshenasfard, M., Esfahany, M.N., Investigation of nanofluids heat transfer in a ribbed microchannel heat sink using single-phase and multiphase CFD models, *International Communications in Heat and Mass Transfer*, 68, 2015, 122-129.
- [50] Rajabi, A.H., Toghraie, D., Mehmandoust, B., Numerical simulation of turbulent nanofluid flow in the narrow channel with a heated wall and a spherical dimple placed on it by using of single phase and mixture- phase models, *International Communications in Heat and Mass Transfer*, 108, 2019, 104316.
- [51] Li, Z., Shahsavari, A., Niazi, K., Al-Rashed, A.A.A., Rostami, S. Numerical assessment on the hydrothermal behavior and irreversibility of MgO-Ag/water hybrid nanofluid flow through a sinusoidal hairpin heat exchanger, *International Communications in Heat and Mass Transfer*, 115, 2020, 104628.
- [52] Ansys Inc, Fluent User Guide and Fluent Theory Guide, version 14.5.
- [53] navi, S.A., Ramiar, A., Ranjbar, A.A., Turbulent forced convection of nanofluid in a wavy channel using two phase model, *Heat & Mass Transfer*, 50, 2014, 661-671.
- [54] Mukherjee, A., Rout, S., Barik, A.K., Heat transfer and entropy generation analysis of a protruded surface in presence of a cross-flow jet using Al₂O₃-water nanofluid, *Thermal Science and Engineering Progress*, 5, 2018, 327-338.

ORCID iD

Bouziane Boudraa  <https://orcid.org/0000-0003-3689-4459>

Rachid Bessaïh  <https://orcid.org/0000-0002-0764-7731>



© 2021 Shahid Chamran University of Ahvaz, Ahvaz, Iran. This article is an open access article distributed under the terms and conditions of the Creative Commons Attribution-NonCommercial 4.0 International (CC BY-NC 4.0 license) (<http://creativecommons.org/licenses/by-nc/4.0/>).

How to cite this article: Boudraa B., Bessaïh R. Turbulent Forced Convection and Entropy Generation of Impinging Jets of Water-Al₂O₃ Nanofluid on Heated Blocks, *J. Appl. Comput. Mech.*, 7(4), 2021, 2010-2023. <https://doi.org/10.22055/JACM.2020.35216.2599>

Publisher's Note Shahid Chamran University of Ahvaz remains neutral with regard to jurisdictional claims in published maps and institutional affiliations.

